

# CFD Analysis of Heat Transfer Enhancement in a Flat-Plate Solar Collector with Different Geometric Variations in the Superficial Section

William Quitiaquez<sup>a\*</sup>, José Estupinán-Campos<sup>a</sup>, César Nieto-Londoño<sup>b</sup>, C.A. Isaza-Roldán<sup>b</sup>,  
Patricio Quitiaquez<sup>a</sup>, Fernando Toapanta-Ramos<sup>a</sup>

<sup>a</sup> Mechanical Engineering, Renewable Energies and Mechanical Implementation of SMEs Research Group GIERIMP, Universidad Politécnica Salesiana, Av. Rumichaca Ñan and Av. Moran Valverde, Quito, 170108, Ecuador

<sup>b</sup> Energy and Thermodynamic Research Group, Universidad Pontificia Bolivariana, Medellín, 050031, Colombia

Corresponding author: \*wquitiaquez@ups.edu.ec

**Abstract**—Nowadays, there is an increasing need for improving the inefficient ways for obtaining thermal energy from renewable sources to fulfil the industrial and typical needs in heat transfer processes that may be covered using solar assisted heat pumps due to their appropriate performance in the thermal energy transfer process. To improve the efficiency of the collector/evaporator by increasing the heat flux to the refrigerant, in this research, a numerical and computational fluid dynamics (CFD) analysis is conducted with geometrical variations in the surface section of a collector/evaporator. The performance was compared to the results of a base case, replicating its limit and environmental conditions such as the initial temperature of 5.5 °C, incident solar radiation of 464.1 W·m<sup>-2</sup>, the operating temperature of 17.6 °C and other parameters. The surface geometrical variations involved in this study show a surface area similar to the base case. However, different lengths of the fluid path were considered due to the new geometrical shapes represented with less thermal resistances and correct distribution of the fluid in the collector/evaporator, obtaining temperature variations of 3.78, 5.47, 5.56 °C and a maximum value of 5.63 °C, including the corresponding variation of the heat flux. Considering the geometric changes in the superficial section of a flat-plate solar collector, it is possible to implement these variations in different kinds of heat exchangers in order to analyze the efficiency in these devices and the impact in the global systems where the heat exchangers are used.

**Keywords**— Energy; heat; surface section; efficiency; temperature.

Manuscript received 21 Apr. 2021; revised 30 Jun. 2021; accepted 29 Aug. 2021. Date of publication 31 Oct. 2021.  
IJASEIT is licensed under a Creative Commons Attribution-Share Alike 4.0 International License.



## I. INTRODUCTION

Due to the increment in energy consumption in the development of different sectors, an increase in the consumption of fossil energy sources has been generated, and this has produced a negative effect on the environment [1], [2]. Due to this situation, different technologies that employ solar energy are currently analyzed to improve efficiencies and reduce carbon dioxide (CO<sub>2</sub>) generation [3]. The direct-expansion solar-assisted heat pump (DX-SAHP) system is used in heating applications of different fluids that employ refrigerants as working fluids in the vapor compression refrigeration cycle because they have a series of thermodynamic, physicochemical and environmentally acceptable (low flammability and toxicity) properties [4].

The DX-SAHP systems can be utilized in different fields with reduced energy consumption, as stated by Ji *et al.* [5]. They consider different design and operation factors, such as the relative humidity, which, when increased from 70 to 90 %, causes an increment of 16.3 % in the COP of the uncovered flat plate device. Combariza *et al.* [6] state that different parameters influence the performance of a heat pump using numerical models that consider continuity, momentum and energy conservation equations to vary values of pressure, velocity, heat flux, among others, despite exhibiting errors smaller than 6 %. These values show their validity when being contrasted with experimental results achieving a reduction of 60.2 % in electrical consumption when the temperature of sanitary water increases from 25 a 32 °C, compared to the same process with electrical resistances.

To improve the performance in devices that use solar radiation, such as flat-plate collectors, investigations using

new materials with experimental and numerical validation are being carried out as can be appreciated in the research of Zhou *et al.* [7] used this method in a conventional solar collector and achieved an increase of 11.3 % in the efficiency of the device, considering 20 °C as ambient temperature.

The research conducted is focused on improving the use of solar energy. It involves handling the heat flux, where the temperatures achieved are validated through the use of a CFD software such as the analysis performed by Panchal and Patel [8], where the geometry and meshed of the construction model are carried out using software for different applications such as solar collectors, drying chambers, agricultural domes, among others. In further studies, the CFD validation is developed with software, which achieves acceptable results in the design and generates an improvement in compact heat exchangers, as shown in the study by Abeykoon [9], where it is observed that this type of validation may be used for different design options without requiring to build prototypes that employ working fluids with different thermodynamic properties.

In order to improve the efficiency of a solar collector (flat-plate), which absorbs energy in a solar-assisted direct-expansion heat pump, this component uses the incident solar radiation to complete the working fluid phase change into superheat vapor, Ma *et al.* [10] carried out a simulation in which the COP of a DX-SAHP is larger than the corresponding to a conventional heat pump system. To reach the superheated state, the refrigerant temperature increases from 2 to 3 °C.

Saffarian *et al.* [11] modified the flow direction in a flat-plate solar collector to increase the convection heat transfer coefficient. They apply three geometries, namely U-shaped, wavy, and spiral, and solve the steady-state continuity, momentum, and energy equations; they use water with copper oxide and aluminum nanofluids as working fluids. Results show an increase of 78.25 % in the heat transfer coefficient when using wavy pipelines and the water with copper oxide nanofluid. In the research conducted by Yao *et al.* [12], uncovered flat-plate collector/evaporator is studied at -10 °C and with solar irradiation of 500 W·m<sup>-2</sup>, reaching a value of 4 as a coefficient of performance.

The objective of the present investigation is to investigate the effect of different surface shapes that may be implemented for the path of the pipeline through which the refrigerant will circulate in a collector/evaporator constituent of a DX-SAHP system. For this purpose, a mathematical description of the system governed by various equations is presented, and a CFD analysis is conducted about the effect of new configurations on the surface area of the pipeline.

## II. MATERIALS AND METHOD

The present study conducts a comparative analysis of the increment of the heat transfer in a collector/evaporator using R600a refrigerant as a working fluid. This study considers as reference the experimental parameters of a base model of the heat exchanger presented in the investigation of Quitiaquez *et al.* [13], [14], which are shown in Table 1. A numerical and CFD analysis is conducted, generating proposals that consider changes in the pipeline arrangement to obtain better results regarding heat transfer, using an output temperature more extensive than the initial model shown in Fig. 1.

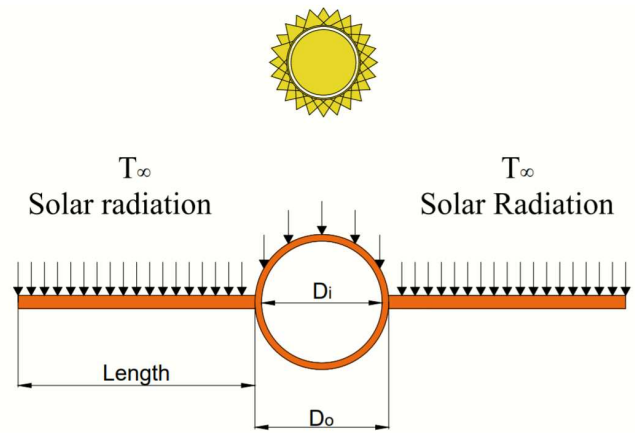


Fig. 1 Original model of the collector/evaporator [15]

### A. Experimental parameters

The results obtained with the initial case to analyze the different models proposed and compared, it is necessary to consider the conditions under which the base model was developed to use them as parameters in the proposed analyses, as seen in Table 1.

TABLE I  
INPUT CONDITIONS FOR THE UNCOVERED FLAT PLATE SOLAR COLLECTOR

AMBIENT TEMPERATURE (T <sub>∞</sub> )	INCIDENT SOLAR RADIATION (G)	INPUT TEMPERATURE (T <sub>4</sub> )	CROSS-SECTION (A)
17.6 °C	464.1 (W·M <sup>-2</sup> )	5.5 (°C)	1.134·10 <sup>-5</sup> (M <sup>2</sup> )

The analysis was conducted in a collector/evaporator that has a horizontal collector plate and a conduit that passes through it in the central region in model 1, as can be seen in Fig. 2 in a central cut view; however, its distribution changes in models 2, 3 and 4.

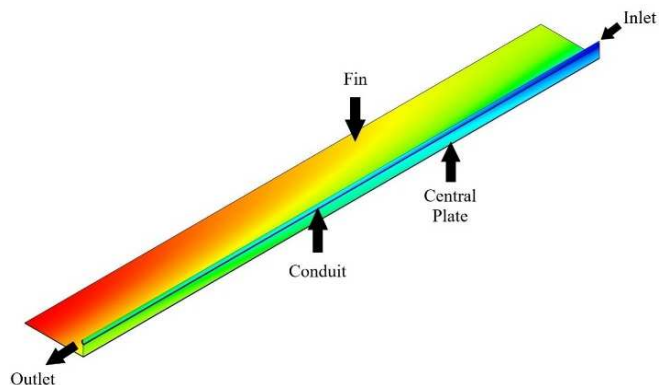


Fig. 2 Original model of the collector/evaporator

### B. CFD Analysis

To conduct simulations with different parameters and their influence in the movement of fluids, the software for CFD analysis performs calculations that are governed by equations that represent the conservation of continuity (mass), energy, and momentum (when there is heat flux), described in (1), (2) and (3), respectively [1], [7].

$$\frac{\partial \rho}{\partial t} + \nabla \cdot (\rho \vec{v}) = S_m \quad (1)$$

$$\frac{\partial}{\partial t} (\rho E) + \nabla \cdot [\vec{V}(\rho E + P)] = -\nabla \cdot (\sum_j h_j J_j) + S_h \quad (2)$$

$$\frac{\partial}{\partial t} (\rho \vec{V}) + \nabla \cdot (\rho \vec{V} \vec{V}) = -\nabla P + \nabla \cdot \left\{ \mu \cdot \left[ (\nabla \vec{V} + \nabla \vec{V}^T) - \frac{2}{3} \nabla \cdot \vec{V} I \right] \right\} + \rho \vec{g} + \vec{F} \quad (3)$$

In the case of conducting analyses that involve fluids with phase change, the required calculations are governed by equations specific for these models that similarly represent the conservation of mass, energy, and momentum considering the phases related, as it is seen in 4, 5, and 6, respectively, which represent the equations of the Eulerian model used in the present research [16], [17].

$$\frac{\partial}{\partial t} (\alpha_q \rho_q) + \nabla \cdot (\alpha_q \rho_q \vec{v}_q) = \sum_{p=1}^n (\dot{m}_{pq} - \dot{m}_{qp}) + S_q \quad (4)$$

$$\frac{\partial}{\partial t} (\alpha_q \rho_q h_q) + \nabla \cdot (\alpha_q \rho_q \vec{u}_q h_q) = \alpha_q \frac{\partial p_q}{\partial t} + \dots \\ \dots \bar{\tau}_q : \nabla \vec{u}_q - \nabla \cdot \vec{q}_q \cdot S_q + \sum_{p=1}^n (Q_{pq} + \dot{m}_{pq} h_{pq} - \dot{m}_{qp} h_{qp}) \quad (5)$$

$$\frac{\partial}{\partial t} (\alpha_q \rho_q \vec{v}_q) + \nabla \cdot (\alpha_q \rho_q \vec{v}_q \vec{v}_q) \\ = -\alpha_q \nabla P + \nabla \cdot \bar{\tau}_q + \dots \\ \dots \alpha_q \rho_q \vec{g} + \sum_{p=1}^n [K_{pq} (\vec{v}_p - \vec{v}_q) + \dot{m}_{pq} \vec{v}_{pq} - \dot{m}_{qp} \vec{v}_{qp}] \dots \\ \dots + (\vec{F}_q + \vec{F}_{lift,q} + \vec{F}_{wl,q} + \vec{F}_{vm,q} + \vec{F}_{td,q}) \quad (6)$$

1) *Turbulence model*: The flow regime in the CFD analysis is considered when involving the required turbulence models in the simulation. In the case of turbulent flows, the most widely used models are k-ε, with its governing 7 and 8 and k-ω, which exhibit high fidelity in their results for the development of the fluid. In the particular case of the k-ε model, it requires a smaller computational expense [18].

$$\frac{\partial}{\partial t} (\rho k) + \frac{\partial}{\partial x_i} (\rho k u_i) = \frac{\partial}{\partial x_j} \left[ \left( \mu + \frac{\mu_t}{\sigma_k} \right) \frac{\partial k}{\partial x_j} \right] + \dots \\ \dots G_k + G_b - \rho \varepsilon - Y_M + S_k \quad (7)$$

$$\frac{\partial}{\partial t} (\rho \varepsilon) + \frac{\partial}{\partial x_i} (\rho \varepsilon u_i) = \frac{\partial}{\partial x_j} \left[ \left( \mu + \frac{\mu_t}{\sigma_\varepsilon} \right) \frac{\partial \varepsilon}{\partial x_j} \right] + \dots \\ \dots C_{1\varepsilon} \frac{\varepsilon}{k} (G_k + C_{3\varepsilon} G_b) - C_{2\varepsilon} \rho \frac{\varepsilon^2}{k} + S_\varepsilon \quad (8)$$

2) *Mesh*: Due to the variety of models proposed, it is required to carry out an independent meshed in each case to validate its modeling. However, since the heat fluxes in the interface are calculated by integration, it is required a refined meshed in this zone in all models proposed, as can be seen in Fig. 3, obtaining an average value of skewness smaller than 0.25 and average orthogonal quality of 0.8 [19].

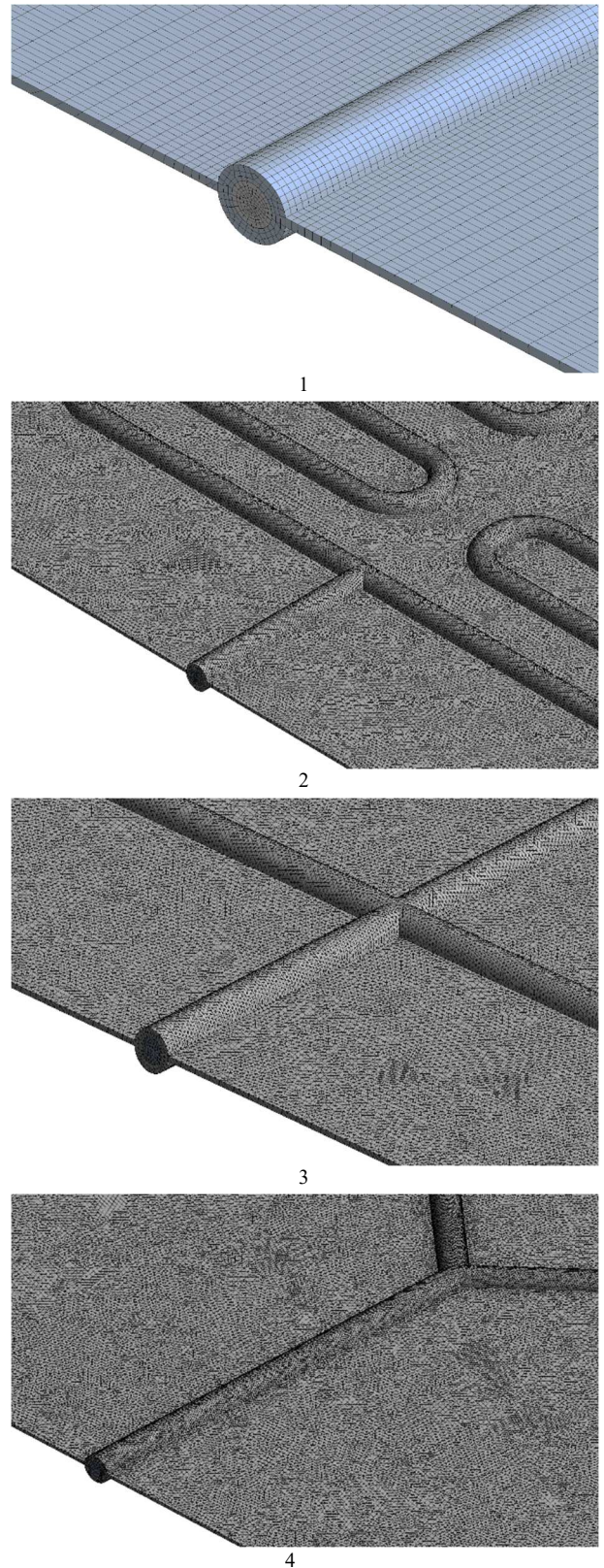


Fig. 3 Meshed in the collector/evaporator in models 1 – 4.

### III. RESULTS AND DISCUSSION

The results obtained in this investigation come from a numerical analysis that considered parameters such as mass flow, fluid quality, incident solar radiation, input, and ambient temperature, among others. The purpose is to generate a comparative analysis of the influence of different surface sections and how they can increase the heat flux in a collector/evaporator.

#### A. Validation

In order to validate the numerical analysis with the mathematical algorithm generated and the CFD models. The experimental results were obtained with a built model [13] that employed conditions similar to the ones considered in the numerical studies, like the research work by Duarte et al. [20] and Ma *et al.* [10]. It obtained errors of 0.11 and 1.12 % respectively, comparing the outlet temperature obtained in the experimental process. The simulated result in the base case is subject to the divergence of the values, with the data presented in Table 2 [12]. Besides, as presented in some research, CFD analyses can be realized in steady and transient states or with steady considerations to obtain useful values in the investigation processes [20], [21].

TABLE II  
OUTPUT TEMPERATURE

OUTPUT TEMPERATURE IN DIFFERENT ANALYSES		
Experimental [13]	CFD	Mathematical algorithm
9.5 °C	9.39 °C	9.51 °C

The output temperature in the CFD analysis for validation considers the value in the central region of a circular pipe, as shown in Fig. 4. The maximum values of 9.5 °C in the region of the interface with the wall.

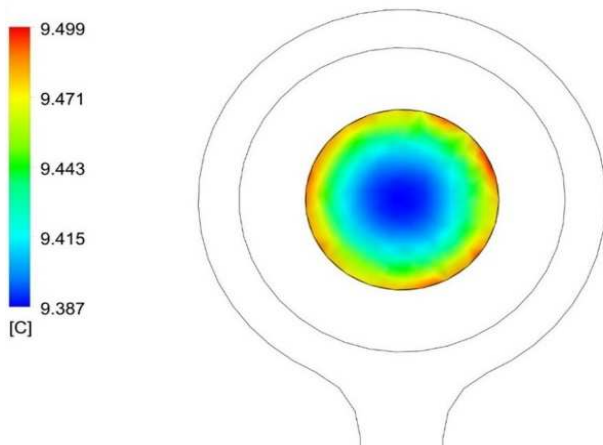


Fig. 4 Output temperature of the CFD analysis

#### B. Results in the surface changes

The increase in the heat flux present in the R600a refrigerant may be determined by the temperature variation between the inlet and the outlet of the working fluid in the heat exchanger, as seen in Fig. 5.

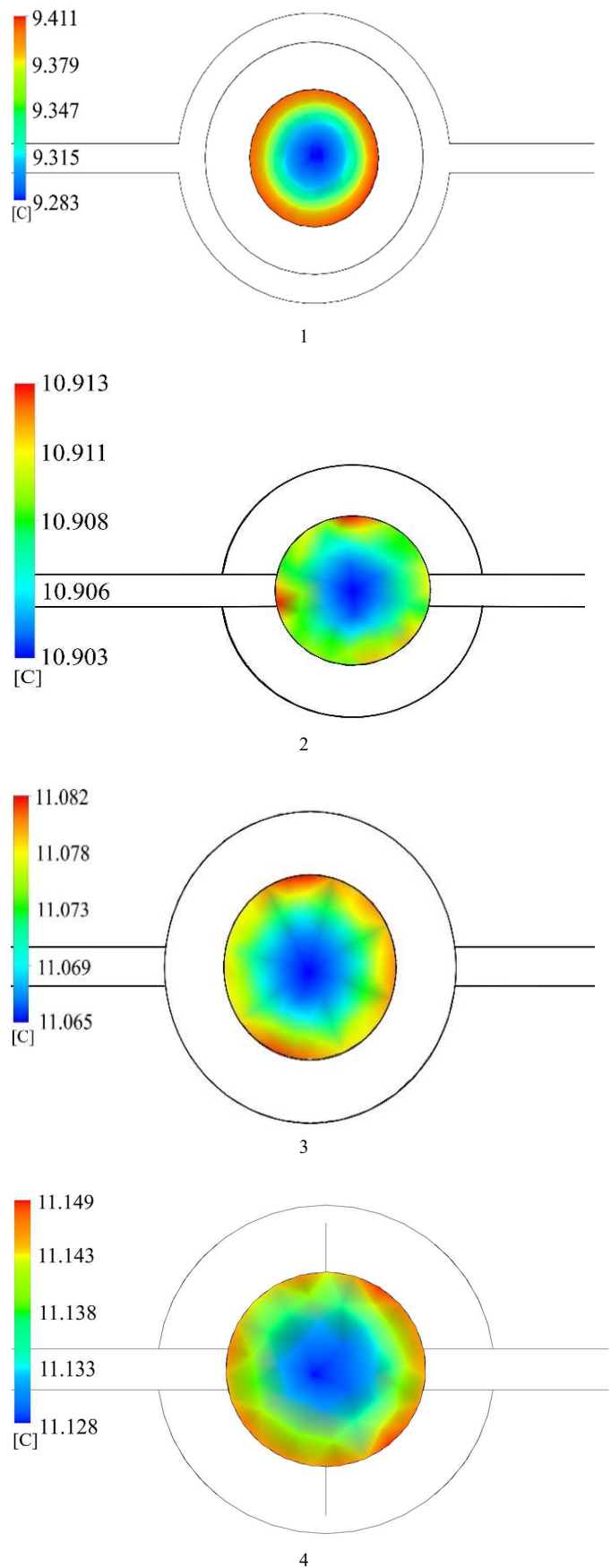


Fig. 5 Output temperature in the collector/evaporator in cases 1 – 4.

The temperature change generated in the proposed models improves the heat exchange process, visible when compared with the output temperature of the base case (O) with a value of 9.5 °C. It results in the central region of 9.28, 10.9, 11.07 and 11.13 °C in models 1, 2, 3, and 4, respectively, leading to the comparative analysis shown in Table 3.

Similarly, this increase may be seen along with the heat exchanger in a region close to the fluid, within the conduit at 0.1 mm of the refrigerant interface wall, as shown in Figures 6, 7, and 8. Fig. 6 shows the temperature increase for Model 1.

TABLE III  
ANALYSIS DATA

Geometry	Model 1		Model 2		Model 3		Model 4	
Arrangement								
Surface area of plate, $A_s$	0.2275		0.2485		0.2318		0.2304	
	CFD	Mat Alg.	CFD	Mat. Alg.	CFD	Mat. Alg.	CFD	Mat. Alg.
Range of plate surface temperature, $T_s$	8.98-13.39	-	6.93-11.81	-	7.91-12.32	-	8.11-13.46	-
Average plate surface temperature, $T_s$	11.18	9.98	9.37	11.40	10.12	11.60	10.78	11.64
Maximum output temperature, $T_l$	9.41	9.41	10.91	10.90	11.08	11.10	11.149	11.15
Variation between values of output temperature of the collector/evaporator, $\Delta T_l$	0.001		0.010		0.02		0.01	
Useful heat flux, $\dot{Q}_U$	24.25		33.72		35		35.31	

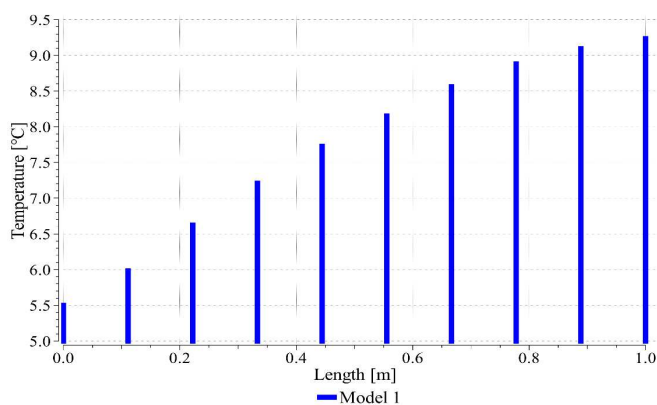


Fig. 6 Temperature along the collector/evaporator in model 1

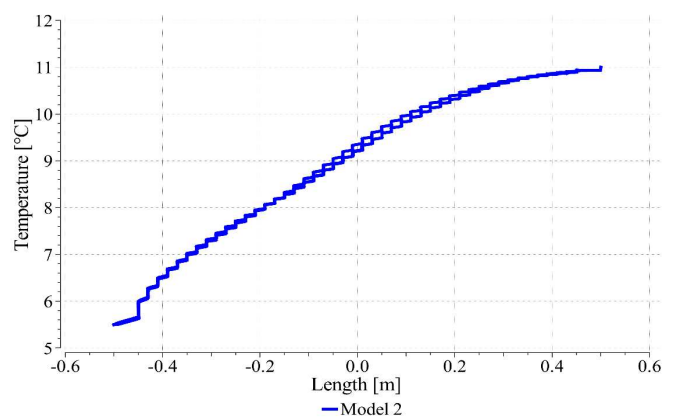


Fig. 7 Temperature along the collector/evaporator in model 2

Similarly, the increasing temperature trend may be seen in model 2, where there is a temperature variation of 5.47 °C between the inlet and outlet of the heat transfer device, as seen in Figure 7.

The increase in heat flux visible in models 3 and 4 results in various temperatures along with the collector/evaporator of 5.56 and 5.63 °C, respectively, revealing a greater heat flux in the heat exchanger, as shown in Fig. 8 (A and B).

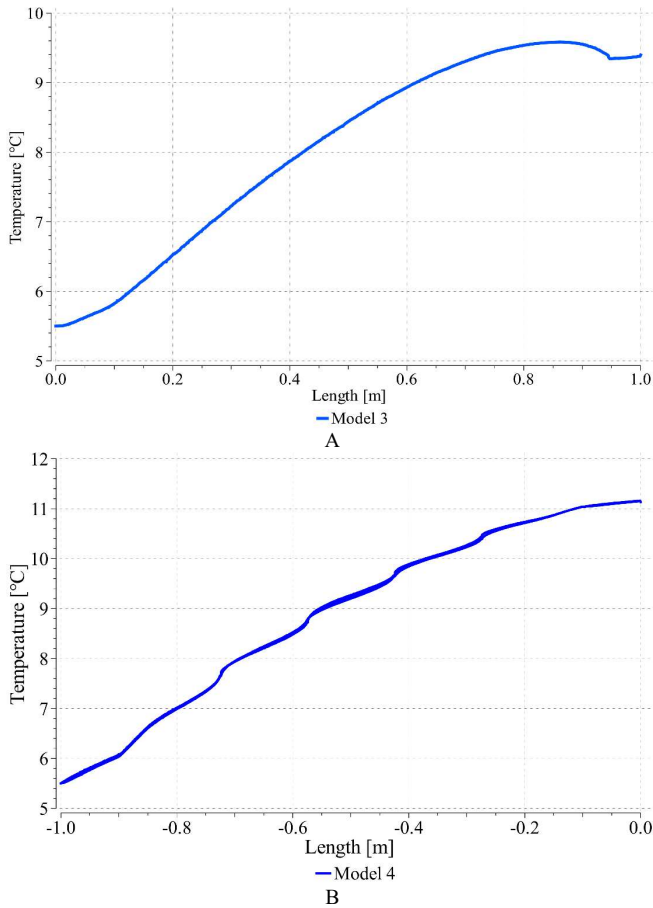


Fig. 8 Temperature along with the collector/evaporator in models 3 and 4

Similarly, a higher surface temperature may be seen in the flat-plate solar collector external regions, indirectly showing the heat flux of the areas with higher temperatures to the areas with a lower temperature that are in contact with the refrigerant path seen in Fig. 9.

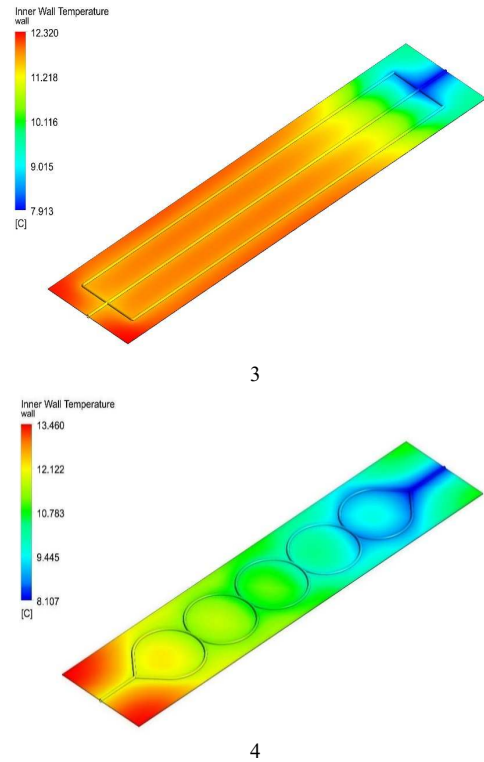
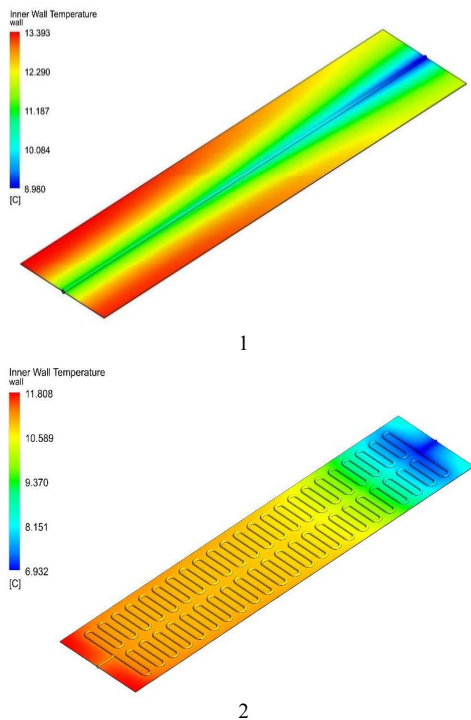


Fig. 9 Surface temperature in the collector/evaporator in models 1 – 4

#### IV. CONCLUSIONS

In the present research work, a numerical simulation was carried out utilizing the application of a mathematical algorithm generated and a CFD analysis of a collector/evaporator, obtaining a relative error between experimental and simulated results smaller than 1.5 % in the validation process, from which the following conclusions were obtained. The temperature increase present in the refrigerant that circulates in the collector/evaporator represents the increase in the heat flux with temperature variations in the central region of the collector/evaporator of 3.78, 5.4, and 5.57 °C in models 1, 2, and 3, respectively, where it is seen how a more considerable heat flux to the R600a refrigerant is generated when increasing the length of the conduit along with the collector plate. The direction of the heat flux in the heat transfer device is seen with the temperature difference in the heat exchanger with minimum values in the central region of the conduit, and maximum surface temperatures of 13.39, 11.81, 12.32, and 13.46 °C for models 1, 2, 3 and 4, respectively, at the most distant regions of the collector plate. The larger output temperature in the R600a refrigerant appears in model 4, with 11.13 °C in the central region of the conduit, resulting in a temperature increase of 5.63 °C along with the collector/evaporator, with a ring-shaped distribution of the conduit in the device and a more considerable length compared to the first model analyzed.

#### NOMENCLATURE

t	time	s
V	velocity	m·s <sup>-1</sup>
v	velocity	m·s <sup>-1</sup>

u	velocity	$\text{m}\cdot\text{s}^{-1}$
S	source	$\text{kg}\cdot\text{m}^{-3}\cdot\text{s}^{-1}$
P	pressure	Pa
T	temperature	K, °C
F	force	N
E	total energy	J
h	enthalpy	$\text{kJ}\cdot\text{kg}^{-1}$
J	mass flow; diffusion flow	$\text{kg}\cdot\text{m}^{-2}\cdot\text{s}^{-1}$
$\dot{m}$	mass transference	$\text{kg}\cdot\text{s}^{-1}$
F	force	N
k	kynetic energy turbulence	$\text{m}^2\cdot\text{s}^{-2}$
x	axial coordinate	
G	energy generation	
$F_q$	external body force	N
$F_{lift,q}$	elevation force	N
$F_{wl,q}$	virtual mass force	N
$F_{td,q}$	dispersion turbulence force	N
Greek letters		
$\rho$	density	$\text{kg}\cdot\text{m}^{-3}$
$\mu$	dynamic viscosity	cP
$\nabla$	grad operator	
$\alpha$	volume fraction	
$\bar{\tau}_q$	Phase tension tensor	Pa
$\mathcal{E}$	Dissipation rate	$\text{m}^2\cdot\text{s}^{-3}$
Subscripts		
m	mass	
h	defined energy	
rq	reference phase	
q	q phase	
p	p phase	
pq	transference from p phase to q phase	
qp	transference from q phase to p phase	
t	turbulence	
k	kynetic turbulence	
b	flotability kynetic turbulence	
e	equilibrium	

#### ACKNOWLEDGMENT

We are grateful to Universidad Politécnica Salesiana and Universidad Pontificia Bolivariana.

#### REFERENCES

- [1] Z. Badiei, M. Eslami, and K. Jafarpur, "Performance improvements in solar flat plate collectors by integrating with phase change materials and fins: A CFD modeling," *Energy*, vol. 192, 2020.
- [2] S. Vaishak and P. V. Bhale, "Photovoltaic/thermal-solar assisted heat pump system: Current status and future prospects," *Sol. Energy*, vol. 189, no. November 2018, pp. 268–284, 2019.
- [3] L. Evangelisti, R. De Lieto Vollaro, and F. Asdrubali, "Latest advances on solar thermal collectors: A comprehensive review," *Renew. Sustain. Energy Rev.*, vol. 114, no. August, 2019.
- [4] F. Gorozabel Chata and T. Carbonell Morales, "Diseños experimentales aplicados a una bomba de calor de expansión directa con energía solar," *Ing. Mecánica*, vol. 20, no. 2, pp. 160–168, 2018.
- [5] W. Ji, J. Cai, J. Ji, and W. Huang, "Experimental study of a direct expansion solar-assisted heat pump (DX-SAHP) with finned-tube evaporator and comparison with conventional DX-SAHP," *Energy Build.*, vol. 207, 2020.
- [6] H. M. C. Bastos, P. J. G. Torres, and C. E. Castilla Álvarez, "Numerical simulation and experimental validation of a solar-assisted heat pump system for heating residential water," *Int. J. Refrig.*, vol. 86, pp. 28–39, 2018.
- [7] L. Zhou, Y. Wang, and Q. Huang, "CFD investigation of a new flat plate collector with additional front side transparent insulation for use in cold regions," *Renew. Energy*, vol. 138, pp. 754–763, 2019.
- [8] H. N. Panchal and N. Patel, "ANSYS CFD and experimental comparison of various parameters of a solar still," *Int. J. Ambient Energy*, vol. 39, no. 6, pp. 551–557, 2018.
- [9] C. Abeykoon, "Compact heat exchangers – Design and optimization with CFD," *Int. J. Heat Mass Transf.*, vol. 146, 2020.
- [10] K. Ma, Z. Wang, X. Li, P. Wu, and S. Li, "Structural optimization of collector/evaporator of direct-expansion solar/air-assisted heat pump," *Alexandria Eng. J.*, vol. 60, no. 1, pp. 387–392, 2021.
- [11] M. R. Saffarian, M. Moravej, and M. H. Doranehgard, "Heat transfer enhancement in a flat plate solar collector with different flow path shapes using nanofluid," *Renew. Energy*, vol. 146, pp. 2316–2329, 2020.
- [12] J. Yao, S. Zheng, D. Chen, Y. Dai, and M. Huang, "Performance improvement of vapor-injection heat pump system by employing PVT collector/evaporator for residential heating in cold climate region," *Energy*, vol. 219, 2021.
- [13] W. Quitiaquez *et al.*, "Analysis of the thermodynamic performance of a solar-assisted heat pump using a condenser with recirculation," *Energia*, vol. 16, no. 2, pp. 111–125, 2020.
- [14] W. Quitiaquez, J. Estupinan-Campos, C. A. Isaza-Roldan, C. Nieto-Londono, P. Quitiaquez, and F. Toapanta-Ramos, "Numerical simulation of a collector/evaporator for direct-expansion solar-assisted heat pump," *2020 IEEE Andescon, Andescon 2020*, 2020.
- [15] W. Quitiaquez, J. Estupinan-Campos, C. A. Isaza Roldán, F. Toapanta-Ramos, and A. Lobato-Campoverde, "Análisis numérico de un sistema de calentamiento de agua utilizando un colector solar de placa plana," *Ingenius*, no. 24, pp. 97–106, 2020.
- [16] H. Shi, M. Li, P. Nikrityuk, and Q. Liu, "Experimental and numerical study of cavitation flows in venturi tubes: From CFD to an empirical model," *Chem. Eng. Sci.*, vol. 207, pp. 672–687, 2019.
- [17] T. Luo, C. Yu, R. Liu, M. Li, J. Zhang, and S. Qu, "Numerical simulation of LNG release and dispersion using a multiphase CFD model," *J. Loss Prev. Process Ind.*, vol. 56, no. August 2017, pp. 316–327, 2018.
- [18] A. Aghagoli and M. Sorin, "Thermodynamic performance of a CO2 vortex tube based on 3D CFD flow analysis," *Int. J. Refrig.*, vol. 108, pp. 124–137, 2019.
- [19] Z. Wang and M. Liu, "Semi-resolved CFD-DEM for thermal particulate flows with applications to fluidized beds," *Int. J. Heat Mass Transf.*, vol. 159, 2020.
- [20] W. M. Duarte, T. F. Paulino, J. J. G. Pabon, S. Sawalha, and L. Machado, "Refrigerants selection for a direct expansion solar assisted heat pump for domestic hot water," *Sol. Energy*, vol. 184, no. April, pp. 527–538, 2019.
- [21] M. Granda, M. Trojan, and D. Taler, "CFD analysis of steam superheater operation in steady and transient state," *Energy*, vol. 199, 2020.
- [22] D. W. Theobald, B. Hanson, M. Fairweather, and P. J. Heggs, "Implications of hydrodynamics on the design of pulsed sieve-plate extraction columns: A one-fluid multiphase CFD model using the volume of fluid method," *Chem. Eng. Sci.*, vol. 221, 2020.